Estimation of Multivariate Observation-Error Statistics for AMSU-A Data

VADIM E. GORIN AND MIKHAIL D. TSYRULNIKOV

HydroMeteorological Center of Russia, Moscow, Russia

(Manuscript received 1 July 2010, in final form 9 April 2011)

ABSTRACT

Advanced Microwave Sounding Unit A (AMSU-A) observation-error covariances are objectively estimated by comparing satellite radiances with radiosonde data. Channels 6–8 are examined as being weakly dependent on the surface and on the stratosphere above the radiosonde top level. Significant horizontal, interchannel, temporal, and intersatellite correlations are found. Besides, cross correlations between satellite and forecast (background) errors (largely disregarded in practical data assimilation) proved to be far from zero. The directional isotropy hypothesis is found to be valid for satellite error correlations. Dependencies on the scan position, the season, and the satellite are also checked. Bootstrap simulations demonstrate that the estimated covariances are statistically significant. The estimated correlations are shown to be caused by the satellite errors in question and not by other (nonsatellite) factors.

1. Introduction

In the past, (in situ) meteorological observations were scarce but accurate (more accurate than the background) and had more or less mutually independent errors. All we needed to know to optimally interpolate the observational information to analysis grid points was observation-error variances and background-error covariances. Now, the situation is different. Satellite observations are comparable with the background both in accuracy and numbers. In addition, satellite observations, like the background, can have correlated errors due to state-dependent imperfections in their observation operators. We may expect multivariate correlations: spatial, temporal, interchannel, intersatellite, intersensor, and others. All these factors make satellite information closer, in its basic properties, to the background than to conventional in situ observations. Therefore, it is likely that satellite *error statistics* are now as important for data assimilation as the widely used background-error statistics.

It has been shown that if spatial satellite error correlations do exist, then their neglect can have detrimental impact on the analysis (see Liu and Rabier 2003; Dando et al. 2007). However, so far various correlations of satellite errors have been largely disregarded in operational systems. As a compensation for this neglect, data thinning together with error variance inflation are normally applied (e.g., Okamoto et al. 2005; Dando et al. 2007; Bormann and Bauer 2010).

Investigations into whether or not satellite error correlations are actually present are not numerous. Bormann et al. (2003) and Le Marshall et al. (2008) showed significant error correlations for satellite wind (atmospheric motion) data. As for satellite radiances, interchannel correlations were found by Garand et al. (2007) and Stewart et al. (2009). Objective estimation of spatial correlations was addressed, to the best of our knowledge, only by Bormann and Bauer (2010), who report on just weak correlations for Advanced Microwave Sounding Unit A (AMSU-A) data, which are the subject of the present article.

The recent results by Bormann and Bauer (2010) were obtained by comparison of satellite data and forecast fields under the hypothesis that there are no cross correlations between satellite and background errors. However, we argue that spatial observation-error correlations should be associated with such cross correlations. Indeed, if satellite errors correlate in space, they do, most likely, correlate also in time. On the other hand, short-term forecast errors also do, certainly, correlate in time with errors of initial forecast data (i.e., analysis errors). Analysis errors, in turn, correlate with observation errors because any state-of-the-art analysis relies heavily on satellite data,

Corresponding author address: M. D. Tsyrulnikov, HydroMeteorological Center of Russia, 11-13 B.Predtechensky Lane, 123242 Moscow, Russia.
E-mail: tsyrulnikov@mecom.ru

DOI: 10.1175/2011MWR3554.1

especially in the upper part of the atmosphere (for now, on AMSU-A observations, to a large extent). These three correlations (temporal correlation of satellite errors, temporal correlation of forecast errors, and cross correlation between analysis errors and satellite observation errors) can (and should) result in simultaneous cross correlation between satellite and forecast errors. If so, spatial satellite error correlations are worth revisiting.

The aim of this research is to estimate various aspects of satellite observation-error statistics for microwave AMSU-A observations known to be one of the most influential sources of observational information for numerical weather prediction to date (e.g., Zapotocny et al. 2008). In particular, spatial auto- and cross-channel covariances, and the distribution of satellite error variance between the correlated and the uncorrelated components are to be estimated. We also study cross correlations between satellite and forecast (background) errors and temporal satellite error correlations, which, both, seem to have attracted little attention so far.

Our basic estimation approach is, as in Bormann et al. (2003), the comparison of satellite and radiosonde observations. Although many AMSU-A frequency channels depend on the state and properties of the surface or the stratosphere beyond the radiosonde altitude range, there are several channels whose observation-operators' supports lie within this range (channels 6–8 over low orography). We confine ourselves to these channels and try to obtain justified estimates for their error covariances only.

The paper is organized as follows. Section 2 introduces the satellite observation error model to be estimated in this study. Section 3 sets up and section 4 presents our estimation methodology. Data used are outlined in section 5. Section 6 describes the estimation results. Statistical significance of the estimated covariances is established in section 7. Section 8 discusses whether our estimation results could be obtained if there were no satellite error correlations. Section 9 explains why our conclusions on AMSU-A error correlations contradict to those by Bormann and Bauer (2010). The main findings of this research are listed in section 10. Implications for practice of data assimilation are briefly discussed in section 11.

2. The satellite observation error model: Theory

In this preparatory section, we discuss how the satellite observation error is defined in the data assimilation context and how it can be decomposed into the uncorrelated and correlated parts.

a. Observation error analysis and definitions

To efficiently assimilate any observations, in particular those of satellites, two things are needed: an observation operator and observation error statistics. The role of the satellite observation operator $\mathcal{H}$ (often called the forward model) is to relate the satellite observations s we are going to assimilate to the atmospheric control vector (the discrete truth at the subsatellite atmospheric column) $\mathbf{X}$ in which we are interested. Given $\mathcal{H}$ and the definition of $\mathbf{X}$, the satellite observation error s' is defined by the observation equation:

$$s = \mathcal{H}(\mathbf{X}) + s' \tag{1}$$

(note that by prime we denote errors).

It is important to stress that this definition depends on the choice of both the control vector (its composition and resolution) and the forward model. If we are going to assimilate s with some particular forward model, then this exact forward model should be used in Eq. (1) to define the observation error.

Specifically, the radiative transfer model (RTTOV) is used as $\mathcal{H}$ in this study. The truth $\mathbf{X}$ is a vertical vector that corresponds to the vertical resolution of RTTOV (43 levels) and to the horizontal resolution of AMSU-A (i.e., 50–100 km). Channels 6–8 in question are virtually not sensitive to atmospheric moisture, so $\mathbf{X}$ is defined here to include only temperatures.

To elaborate on s', let us introduce a hypothetical perfect (or true) forward model $\mathcal{H}_{\text{true}}$ that exactly reproduces the radiation received by the satellite sensor, up to some instrumental noise s'_{inst}. Inevitably, $\mathcal{H}_{\text{true}}$ should depend on the atmospheric state of much greater size than our $\mathbf{X}$. This hypothetical "full" state $\mathbf{X}_{\text{full}}$ includes atmospheric profiles of multiple atmospheric fields with very high (infinite) spatial resolution, involves proper averaging within the sensor's field of view, and accounts for the slant path of the radiation beam received by the sensor.

With this perfect model and full state vector, we can write

$$s = \mathcal{H}_{\text{true}}(\mathbf{X}_{\text{full}}) + s'_{\text{inst}}. \tag{2}$$

Subtracting Eqs. (1) and (2) yields

$$s' = s'_{\text{inst}} - s'_{\text{forw}}, \tag{3}$$

where the forward-model error s'_{forw} is

$$s'_{\text{forw}} := \mathcal{H}(\mathbf{X}) - \mathcal{H}_{\text{true}}(\mathbf{X}_{\text{full}}) \tag{4}$$

(the sign ":=" means "equal by definition"). From this equation, it is clear that the satellite observation error, as defined in the data assimilation context, consists of the two terms: the instrumental error s'_{inst} and the forward-model error s'_{forw}.

Normally, the forward-model error has a systematic component, the bias, which is assessed using a simple bias-correction procedure and subtracted from s. The role of biases in building spatial satellite error correlations is discussed next.

b. State-dependent biases and error correlations

Existing AMSU-A bias-correction schemes address the dependence of the bias on the scan position, latitude, and the local atmospheric state (e.g., Harris and Kelly 2001). Let us consider the state-dependent part of the scheme, which attempts to remove an airmass-dependent error component from s'_{forw} (because s'_{inst} can be deemed to be state independent). This is normally done by introducing a set of state-dependent predictors (typically, some rough characteristics of the vertical distribution of dry and moist air mass and the surface), $\mathbf{X}_{\text{pred}}$, and estimating a regression function $f(\mathbf{X}_{\text{pred}})$ from an archive of differences of satellite data and the background (or radiosondes).

On the other hand, the definition of the forward-model error, Eq. (4), implies—because $\mathbf{X}$ is part of $\mathbf{X}_{\text{full}}$—that

$$s'_{\text{forw}} = g(\mathbf{X}_{\text{full}}), \tag{5}$$

where g is an unknown (because $\mathcal{H}_{\text{true}}$ is unknown) and, presumably, very complicated function of the full state $\mathbf{X}_{\text{full}}$.

Comparing the true state-dependence function $g()$ with what we can devise in practice, $f()$, we observe the fundamental difference in these two functions—spaces, on which they are defined: huge theoretical full space for $g()$ versus tiny ''predictor'' space for $f()$. This difference implies that $f(\mathbf{X}_{\text{pred}})$ has no chance to remove all state-dependent error and so the residual (after state-dependent bias correction) error is inevitably state dependent, too. So, essentially, any practical state-dependent bias-correction scheme can remove only part of the state dependence. The remaining part still depends on the (full) state. This state is, as we know, spatially and temporally correlated, which causes the respective correlations in satellite errors after bias correction.

We remark that horizontally variable state-dependent biases, on the one hand, and horizontal error correlations, on the other hand, are different names of the same phenomenon. A state-dependent bias-correction scheme acts to reduce horizontally varying biases and hence error correlations, but, as discussed above in this section, inevitably, not completely. The remaining correlations are what we estimate in this research.

In the sequel, we assume that satellite data we use are bias corrected.

c. The error model

As discussed, the forward-model error s'_{forw}, even after bias correction, is likely to be spatially (and temporally) correlated. In principle, it can have the uncorrelated (''white'') component as well. The instrumental error s'_{inst} also can have these two error components (uncorrelated and correlated), albeit for other reasons. So, we model the error of bias-corrected satellite observations by the sum of two probabilistically independent components: the uncorrelated one u' and the correlated one c':

$$s' = c' + u'. \tag{6}$$

Here u' is assumed to be uncorrelated: in the horizontal, in time, and with c'. Thus defined, the u' satellite error component appears to be uncorrelated between different channels as well (section 6b). So, we will treat u' as a purely independent noise.

The c' component is, thus, responsible for all the error correlations we consider in this study: spatial, temporal, interchannel, and cross correlations with forecast errors. We also assume that all the white-noise component is due to u', so that c' has continuous (horizontal and temporal) covariance function at zero distance.

As we will see in section 6g, u' appears to be close to the random part of s'_{inst}, so that c' can be associated with s'_{forw} (after bias correction). Note, however, that this association between u' and c' on the one hand and s'_{inst} and s'_{forw} on the other hand cannot be rigorously proven by our purely statistical analysis and so is inevitably speculative.

Thus, it is c' and u' whose statistical characteristics are to be estimated in this study.

3. The estimation setup

In the most general terms, we compare satellite data with collocated radiosonde observations. For comparison and as an auxiliary source of information, we also make use of the short-range (6 h) forecast (analysis background).

a. The error analysis

For each selected satellite channel, we compute the satellite s minus radiosonde r differences $s - r$, where $r := \mathcal{H}(\mathbf{X}^{\text{raob}})$ and $\mathbf{X}^{\text{raob}}$ is the radiosonde profile. The collocation radius is 50 km in space and 2 h in time (this selection is discussed in section 8e). In the same way, we apply $\mathcal{H}$ to the forecast (background) field, getting the forecast f in terms of satellite brightness temperatures; this enables us to examine the differences $f - r$ and $s - f$. All comparisons are made in radiance space, the units being kelvin.

An application of $\mathcal{H}$ to $\mathbf{X}^{\text{raob}}$ involves a vertical interpolation from radiosonde levels to the grid of the radiative transfer model and an application of the radiative transfer model itself. An application of $\mathcal{H}$ to the forecast also involves a horizontal interpolation from the forecast grid to the subsatellite point.

To relate $s - r$, $f - r$, and $s - f$ to the errors in question, we introduce the "reference truth" $t := \mathcal{H}(\mathbf{X})$, the physical-space truth mapped by the exactly known deterministic function $\mathcal{H}$ to radiance space for some particular channel. The introduction of the reference truth (in radiance space) is motivated by Eq. (1), where the satellite error is defined with respect to t. It is worth stressing that our t is *not* the true radiance [$\mathcal{H}_{\text{true}}(\mathbf{X}_{\text{full}})$ in our notation]. Then, by Eqs. (1) and (6),

$$s = t + c' + u'. \tag{7}$$

As for a radiosonde observation, we note that $\mathbf{X}^{\text{raob}}$ differs from $\mathbf{X}$ in several respects. First, they are displaced in the horizontal and in time: within the collocation radius and collocation time window, within the radiosonde launch time uncertainty (about 0.5 h), and as a result of moving by the wind during the radiosonde ascent time. All these factors introduce an error, which can be called the displacement error. Second, the vertical resolution of a radiosonde profile differs from that of $\mathbf{X}$, which introduces a vertical interpolation/averaging error. And finally, $\mathbf{X}^{\text{raob}}$ is subject to the instrumental measurement error, $\delta\mathbf{X}^{\text{raob}}_{\text{inst}}$. The first two radiosonde error sources (i.e., the displacement error and the vertical interpolation/averaging error) can be combined into the representativeness error, $\delta\mathbf{X}^{\text{raob}}_{\text{repr}}$. So,

$$\mathbf{X}^{\text{raob}} = \mathbf{X} + \delta\mathbf{X}^{\text{raob}}_{\text{inst}} + \delta\mathbf{X}^{\text{raob}}_{\text{repr}}. \tag{8}$$

Being converted to radiance space, Eq. (8) gives rise—if $\mathcal{H}$ is only weakly nonlinear, which is the case for the AMSU-A channels 6–8 under investigation—to the equation for the radiosonde error in this study:

$$r = \mathcal{H}(\mathbf{X}^{\text{raob}}) = \mathcal{H}(\mathbf{X}) + \mathbf{H}(\mathbf{X})(\delta\mathbf{X}^{\text{raob}}_{\text{inst}} + \delta\mathbf{X}^{\text{raob}}_{\text{repr}}) = t + r'_{\text{inst}} + r'_{\text{repr}} \equiv t + r', \tag{9}$$

where $\mathbf{H} = \partial\mathcal{H}/\partial\mathbf{X}$ is the forward-model Jacobian. Similarly, $f = t + f'$.

b. The basic assumptions

We assume that radiosonde errors r' (recall, mapped to radiance space) do not correlate with (i) radiosonde errors for different radiosonde ascents, (ii) satellite errors $s' := s - t$, and (iii) forecast errors $f' := f - t$.

We discuss and partly check assumption (i) in section 8.

To justify assumption (ii) we note that radiosonde instrumental error is completely physically independent from satellite error. As for the radiosonde representativeness error, it consists exclusively of subgrid-scale meteorological components, which are absent from the satellite observation because of its field-of-view averaging. So, $(r', s') = 0$.

Assumption (iii) follows from assumption (i) and the fact that imperfections of the forecast model have nothing in common with radiosonde errors. It is important to stress that we allow the cross covariance (s', f') to be nonzero (see the introduction).

We also assume that satellite errors (recall, after bias correction) are homogeneous and isotropic with one caveat: the satellite error variance is allowed to depend on the viewing angle (the scan position). We check this assumption in section 6e.

4. The estimation methodology

First, we estimate variances and interchannel cross covariances for the uncorrelated satellite error components u'. Then, we estimate horizontal and other covariances for the correlated error component. Finally, we estimate uncorrelated and correlated error variances as functions of the scan position.

a. Estimation of the one-point interchannel covariance matrix for u'

For each pair of channels i, j, let us write down the horizontal cross-covariance function for the $s - f$ differences at any horizontal distance ρ:

$$(s_i - f_i, s_j - f_j) = (s'_i - f'_i, s'_j - f'_j) = (u'_i + c'_i - f'_i, u'_j + c'_j - f'_j), \tag{10}$$

where $(,)$ denotes the noncentered covariance $(\xi, \eta) := \mathbb{E}\xi\eta$ for any two real random variables ξ and η ($\mathbb{E}$ stands for mathematical expectation).

In Eq. (10), u' is uncorrelated with c' by definition (section 2c). Further, as u' is uncorrelated in time, the (u', f') covariance can be neglected as well. So, at any distance ρ,

$$(s_i - f_i, s_j - f_j) = (u'_i, u'_j) + (c'_i, c'_j) + (f'_i, f'_j) - (f'_i, c'_j) - (c'_i, f'_j). \tag{11}$$

Now, let us consider the discontinuity of this expression at $\rho = 0$ (i.e., the difference of its value at $\rho = 0$ and its limit as $\rho \to 0$). The (c', c') covariance function is continuous at $\rho = 0$ by definition (section 2c). As for the

forecast-error covariance function (f', f'), we also assume that it is free from the white-noise contribution—for the following reason. Both the gridpoint truth and the forecast should be and normally are regarded as gridcell averages of continuous natural fields and so cannot have subgrid-scale components responsible for the existence of the white-noise component by construction. Then, clearly, the (c', f') cross-covariance function is also continuous at $\rho = 0$, and so the discontinuity in the $(s_i - f_i, s_j - f_j)$ covariance at $\rho = 0$ is exclusively due to the u' error component:

$$(u_i', u_j')|_{\rho=0} = (s_i - f_i, s_j - f_j)|_{\rho=0} - \lim_{\rho\to 0}(s_i - f_i, s_j - f_j)|_{\rho}. \tag{12}$$

Equation (12) is the required estimator for the entries of the one-point u' covariance matrix. The first term in its right-hand side is estimated using the forecast interpolated to the subsatellite point. The second term (the limit) is approximated by an estimate of the $(s - f, s - f)$ horizontal covariance at the smallest available nonzero distance $\rho \simeq 50$ km.

b. The basic estimator for spatiotemporal covariances

Our goal is to estimate spatial and spatiotemporal satellite-error covariances (s', s') and spatial cross covariances between satellite and forecast errors (s', f'). In addition, we wish to have estimates for spatial forecast-error covariances (f', f') (which will be used in section 9).

To achieve this goal, the three types of covariances are, first, related to covariances that can be directly estimated from observations. Second, estimation of all the latter covariances appears to be accomplished with a unified estimator for horizontal covariances.

We note that here, satellite observations with all scan angles are combined in one sample. To simplify the presentation, we describe the estimation technique for autocovariances; its modification for estimation of interchannel covariances is straightforward.

The horizontal satellite-error covariance function (s', s'), as it follows from the above basic assumptions and Eq. (9), equals the covariance function of $s - r \equiv s' - r'$ at any nonzero horizontal distance:

$$(s - r, s - r) = (s' - r', s' - r') = (s', s') = (c', c'), \tag{13}$$

which can be estimated using observations.

Similarly, the horizontal cross-covariance function between satellite and forecast errors coincides with $(s - r, f - r)$. Horizontal forecast-error covariances equal $(f - r, f - r)$ under the above basic assumptions. Finally, spatiotemporal satellite-error covariances are estimated as a set of horizontal satellite-error covariances $(s - r, s^+ - r^+)$, where the superscript $^+$ denotes a time lag, for a number of lags. Thus, all these three types of covariances require estimation of horizontal covariances.

Now, we present our basic estimator on the example of $(s - r, s - r)$ covariances. The horizontal covariances are estimated by averaging $(s_p - r_p)(s_q - r_q)$ over all pairs of collocations (p, q) within bins of distances between the pairs. The algorithm can be outlined as follows. All collocations pairs (p, q) are, first, sorted by the increasing distance ρ_{pq} between their collocation points p and q. Then, the first 30 000 collocation pairs are declared to be placed in the zeroth bin. The covariance for this (and any other) bin is attributed to the center of mass of the bin $\rho_{\rm cm}(0)$ [the same mass is assigned to each collocation pair (p, q)]. The first bin is chosen by placing its center of mass at $\rho_{\rm cm}(1) = 200$ km and choosing 30 000 collocation pairs around it. To obtain the next bin, we start increasing the distance that corresponds to its left boundary starting from the left boundary of the previous bin while preserving the number of collocations constant (=30 000), until its center of mass $\rho_{\rm cm}(2)$ exceeds $\rho_{\rm cm}(1) + 20$ km. The process is repeated to cover the distances up to 3000 km. The bins can, in principle, intersect, which introduces some smoothing.

The basic estimation technique described in this subsection yields useful results, but the estimated autocovariance functions are not guaranteed to be positive definite, the estimates appear to be noisy, and there is a gap in covariances near zero distance (because the radiosonde network is scarce). To cope with these problems, we have devised a spectral-space extension to the basic estimation technique presented in section 4c on the (c', c') example.

c. The spectral-space estimator for horizontal covariances

We expand the (c', c') covariance function for a single channel in the Fourier–Legendre series:

$$(c', c')|_{\rho} = \sum_{n=0}^{N} a_n P_n\left(\cos\frac{\rho}{R_e}\right), \tag{14}$$

where P_n is the Legendre polynomial, N is the maximal wavenumber, $a_n \geq 0$ are the spectral variances (variance spectrum), and R_e is the earth's radius. We found that $N = 100$ is enough to yield stable estimation results (and is consistent with the minimal distance between radiosondes).

It is worth noting that expansion Eq. (14) is the most general form of a limited-resolution continuous covariance function on the sphere [e.g., Yaglom (1987), Eq. (4.191)].

Now, estimation of the (c', c') covariance function is equivalent to the estimation of the spectral variances $\{a_n\}$. The bulk of information we have at our disposal is the set of estimated $(s - r, s - r)$ covariances, C_k ($k = 1, \ldots, K$), at distances ρ_k ranging from about 180 to 3000 km. In its simplest form, our spectral-space estimator minimizes the norm of the difference between "observed" and spectrally modeled covariances:

$$J_c := \sum_{k=1}^{K}\left[C_k - \sum_{n=0}^{N} a_n P_n\left(\cos\frac{\rho_k}{R_e}\right)\right]^2 \to \min, \quad (15)$$

subject to the positive-definiteness condition $a_n \geq 0$ for all n.

The solution to this optimization problem appeared to be somewhat noisy at large distances and not stable enough at small distances. To cope with the former problem, we add to J_c a spectral smoothing term:

$$J_{\text{smo}} := w_{\text{smo}} \sum_{n=1}^{N} (a_n - a_{n-1})^2, \quad (16)$$

with the weight w_{smo} chosen to reduce the covariances beyond the range of 3000 km (so that they are not larger than the estimation error), while changing the covariances in the range of interest, 0–3000 km, as little as possible (the change being again within the estimation error).

To stabilize the solution at $\rho = 0$, we introduce a term that penalizes the misfit between the observed satellite-minus-radiosonde *variance* D_{sr} and its model counterpart:

$$J_0 := w_0\left(D_{\text{sr}} - \sum_{n=0}^{N} a_n - \mathbb{D}u' - \mathbb{D}r'\right)^2. \quad (17)$$

Here we have used that $\mathbb{D}c' = \sum_{n=0}^{N} a_n$. In Eq. (17), we have to specify the weight w_0 and the radiosonde observation error variance $\mathbb{D}r'$ (recall, in terms of satellite brightness temperature). This is done by using a bootstrap-based technique outlined in the appendix. The available information on $\mathbb{D}r'$ is vague, so the role of the J_0 term turns out to be not dramatic in our experiments. Note that $\mathbb{D}u'$ is assumed to be already estimated (section 4a). Our final estimator for horizontal autocovariances is

$$J[\{a_n\}] := J_c + J_{\text{smo}} + J_0 \to \min \quad (18)$$

under the condition $a_n \geq 0$ for $n = 0, \ldots, N$. Estimation of the horizontal cross-channel covariances is performed in a similar way, under the condition of positive definiteness for all 2×2 cross-channel covariance matrices in spectral space.

d. Estimation of scan-dependent satellite error variances

As indicated in section 3b, $\mathbb{D}s'$ is allowed to vary with the scan angle. With a reasonable-size 1-yr data archive, we can estimate only scan-dependent *variances* of both the uncorrelated and correlated satellite error, $\mathbb{D}u'$ and $\mathbb{D}c'$, respectively.

First, $\mathbb{D}u'$ as a function of the scan position is estimated by applying Eq. (12) with $i = j$ for any scan position independently.

Second, $\mathbb{D}c'$ as a function of the scan position is estimated as follows. The $s - r$ variance budget equation:

$$D_{\text{sr}} := \mathbb{D}(s - r) = \mathbb{D}r' + \mathbb{D}u' + \mathbb{D}c', \quad (19)$$

is applied, first, for the whole sample with all scan angles combined. Then, it is applied to the subsample corresponding to the scan position i_{scan}. After that, the two resulting equations are subtracted from each other, yielding the desired estimate:

$$\mathbb{D}c'(i_{\text{scan}}) = \mathbb{D}c' + \mathbb{D}u' - \mathbb{D}u'(i_{\text{scan}}) + D_{\text{sr}}(i_{\text{scan}}) - D_{\text{sr}}. \quad (20)$$

Note that $\mathbb{D}c' = \Sigma_n a_n$ (section 4c), $\mathbb{D}u'$, and $\mathbb{D}u'(i_{\text{scan}})$ are already estimated at this point.

As for the c' error *correlations* for different pairs of scan positions, they can hardly be estimated using satellite-radiosonde collocation data—because any collocation corresponds to just one or two satellite scan positions and the network of collocations separated by the scan angle is, thus, far too sparse to obtain reliable estimation results. Therefore, our satellite observation error model allows for scan-angle dependence of $\mathbb{D}u'$ and $\mathbb{D}c'$ but postulates no such dependence for the correlations of c'—the simplest model that does not contradict to the available data.

5. Data

We use AMSU-A data (channels 6–8) from the National Oceanic and Atmospheric Administration (NOAA) satellite *NOAA-18* and Meteorological Operation satellite *Metop-A* for February–December 2009 and *NOAA-19* for May–December 2009. The observations are quality controlled by limiting their deviations from the background

and from the neighboring pixels. Roughly, 1% of data are rejected thereby. Observations from channel 6 (7) are taken only if the orography is not higher than 1000 (1500) m. The radiative transfer model RTTOV-8.7 (Saunders et al. 1999) is taken as the observation operator.

A flavor of the bias-correction scheme proposed by Harris and Kelly (2001) is applied. Scan correction is performed using background fields, for each scan position separately, in 18 latitude zones. The state-dependent bias correction is performed by subtracting, from raw observations, a linear combination of four predictors: a global constant, two background thicknesses (850–300 and 200–50 hPa) and the observation itself. We note that using the satellite channel measurement itself as a predictor was questioned by some authors, but we found little difference between the results when we use or not use it in our experiments. Either the background or radiosondes are used as a reference to fit the state-dependent bias-correction scheme (both options produce almost the same results in our experiments).

We present results obtained for *NOAA-18*, as the respective results for *Metop-A* and *NOAA-19* are basically the same. The *NOAA-19* data are mentioned in this paper only in the context of estimation of intersatellite correlations.

(The most accurate) Vaisala, Sippican, Meisei, Modem, and Graw radiosonde types are used. Observations at mandatory levels are utilized (all levels are required to be present up to 10 hPa). Radiosonde data undergo a simple background quality control. The statistics are estimated globally, however, more than 95% of radiosonde observations of the above types are located in the Northern Hemisphere, so our results are virtually hemispheric. The summer/winter contrasts are assessed for the Northern Hemisphere only.

The National Centers for Environmental Prediction (NCEP) Global Forecast System (GFS) 6-h forecasts on 26 pressure levels (10–1000 hPa) at horizontal resolution of 1° are used. Forecast and radiosonde temperatures are extrapolated above their top levels and blended with the 40-yr European Centre for Medium-Range Weather Forecasts (ECMWF) Re-Analysis (ERA-40) climatology (Uppala et al. 2005).

6. Estimation results

a. Horizontal autocovariances

Figure 1 (top panel) shows the estimated AMSU-A horizontal covariances. The ''raw covariances'' (left panel) are obtained with our basic estimator (section 4b). The ''smoothed covariances'' (right panel) are estimated by the spectral-space estimator (section 4c).

The covariances' length scales are seen to be quite large, being somewhat larger than those for geostationary satellite atmospheric motion wind (AMV) estimated by Bormann et al. (2003) and substantially larger than for polar AMVs by Le Marshall et al. (2008). Note that we define the length scale as the distance at which the (smoothed) covariance falls to some fraction (e.g., 0.5 or 0.25) of its maximal value at zero distance.

For comparison, Fig. 1 (middle panel) shows the respective estimated background-error covariances, which appear to have comparable (or somewhat larger) length scales and a bit smaller variances as compared to the correlated satellite errors (top panel). The bottom panel of Fig. 1 displays the $(s - f, s - f)$ covariances, to be used in section 9.

b. Interchannel horizontal correlations

First, interchannel covariances for the u' error component are estimated with the technique presented in section 4a. They appear to be negligible, the respective correlations being as small as 0.04 (4%) and less. Note that we switch from covariances (which provide information on both the variance and the correlation) to correlations with the intention to emphasize the spatial (and other) statistical dependency, which is quantified by the correlation.

Second, interchannel horizontal correlations for the correlated satellite error component c' are estimated and presented in Fig. 2.

The interchannel c' correlations appear to be quite high and have horizontal length scales similar to those for autocovariances (cf. Fig. 1). Note, however, that correlations between the nonadjacent channels (6 and 8) are much smaller than correlations between the adjacent channels. This can be understood by taking into account the fact that the channels' weighting functions more significantly overlap for the adjacent channels (the more the overlap, the more similar are, presumably, the respective forward-model imperfections)—see Fig. 3, which displays the rows of the forward-model Jacobian $\mathbf{H}$ computed for an arbitrarily selected point in midlatitudes at an arbitrary date in our archive.

c. Cross correlations between satellite errors and forecast errors

Figure 4 displays cross correlations between (the correlated component of) satellite errors and forecast errors. Again, we see quite broad and large correlations only weakly dependent on the channel number. We would note that to the best of our knowledge, the existence of significant cross correlations between satellite and forecast errors is reported here for the first time.

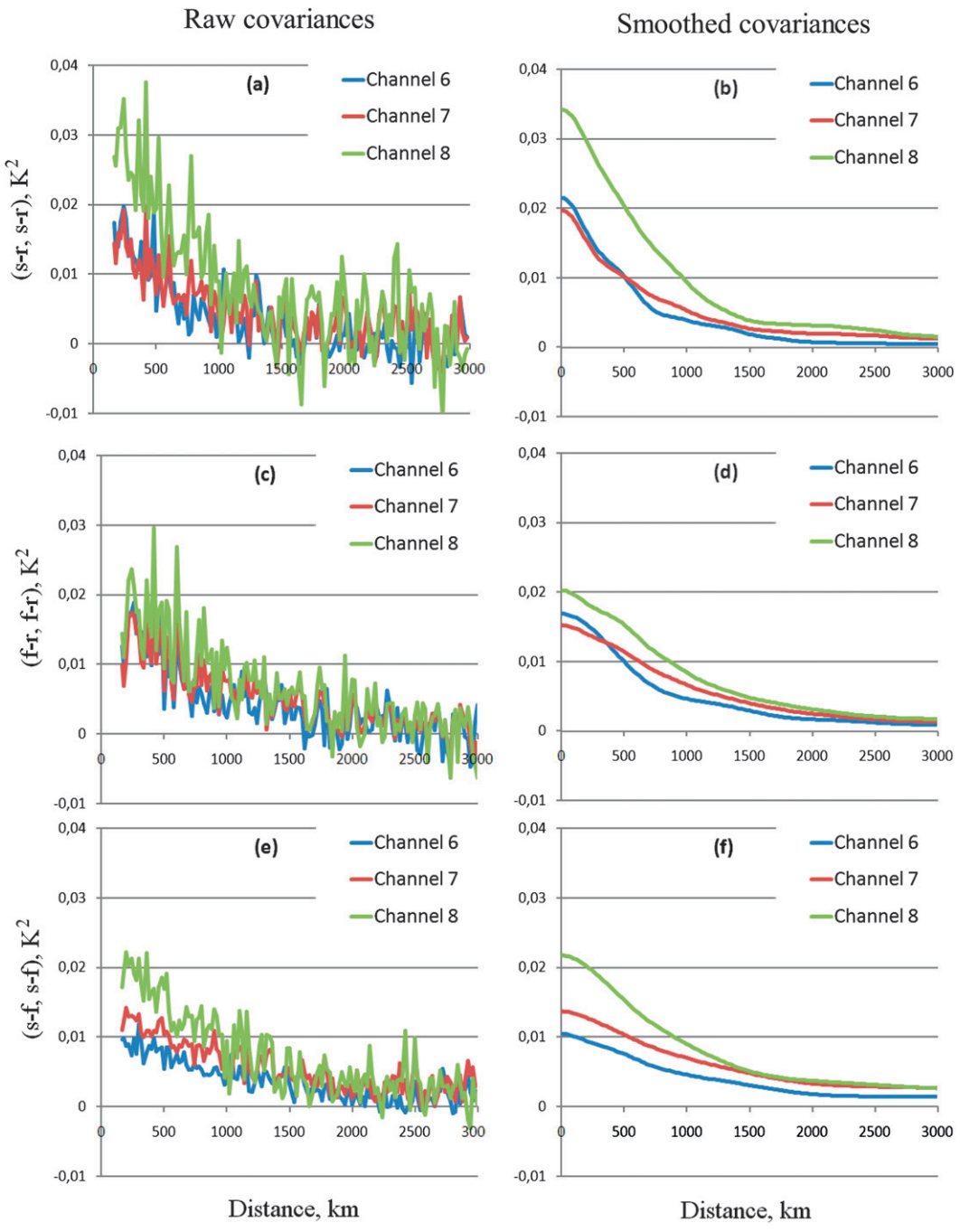

FIG. 1. Horizontal covariances: (a) raw satellite-minus-radiosonde, (b) smoothed satellite-minus-radiosonde, (c) raw background-minus-radiosonde, (d) smoothed background-minus-radiosonde, (e) raw satellite-minus-background (at radiosonde collocations), and (f) smoothed satellite-minus-background (at radiosonde collocations).

These cross correlations are not allowed for in state-of-the-art data assimilation schemes.

d. Scan position dependence

The uncorrelated satellite error variance $\mathbb{D}u'$ turns out to be almost independent on the scan angle (not shown).

Figure 5 displays the estimated $\mathbb{D}c'$ as a function of the scan position. For channel 6, one can see a somewhat irregular dependence, with an increase for small scan angles (this contradicts to the normal practice of rejecting several outermost scan positions in practical schemes). We may hypothesize that this can be caused

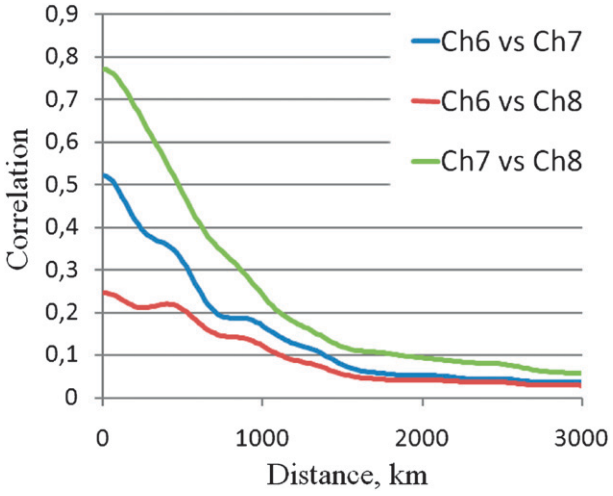

FIG. 2. Interchannel c' cross correlations as functions of distance.

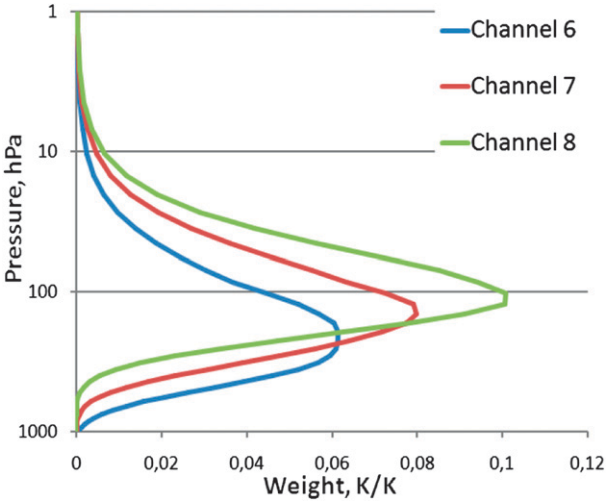

FIG. 3. Channels 6–8 weighting functions with respect to temperature.

by the influence of the underlying surface, larger for smaller zenith angles.

For the other two channels (7 and 8), the scan-position dependence is as expected and exhibits growth of $\mathbb{D}c'$ for several outermost scan positions.

e. *Further results for spatial covariances*

The validity of the local isotropy hypothesis is studied by separating the collocation pairs into two subsamples, with predominantly zonal and predominantly meridional orientation and estimating horizontal ($s - r$, $s - r$) covariances for the two subsamples independently. The resulting covariances appear to be almost the same (not shown), which justifies the directional isotropy hypothesis.

Seasonal contrasts in the satellite covariances are not found: summer (June–August) versus winter (December and February) for radiosondes in the Northern Hemisphere exhibit insignificant differences (not shown).

Covariances for the three satellites with AMSU-A sensors onboard appear to be virtually the same (not shown).

Intersatellite cross covariances between *NOAA-18* and *NOAA-19* are checked and found to be not significantly different from autocovariances for each satellite separately (not shown). This suggests that the satellite error correlation is not due to instrumental errors, but rather due to imperfections in the observation operator.

To verify stability of the estimates, the covariances are computed separately for the two zones: Europe and North America. Qualitatively similar results are obtained (not shown).

We also note that using only the best radiosonde types implies that the radiosonde-satellite collocations we use are located, mostly, in Europe and North America in relatively narrow latitudinal zones. This precludes studying the latitudinal dependence of the satellite error covariances. Without any evidence of latitudinal dependence, we assume that AMSU-A error statistics do not depend on latitude.

f. *Temporal satellite error correlations*

As indicated in section 4b, we estimate here, again, horizontal covariances, but this time with varying time lag. To present the results in a concise fashion and filter out sampling noise, we average the lagged spatial covariances over distances 200–500 km and plot the averages against the time lag. Again, we present correlations to make the degree of temporal statistical dependence

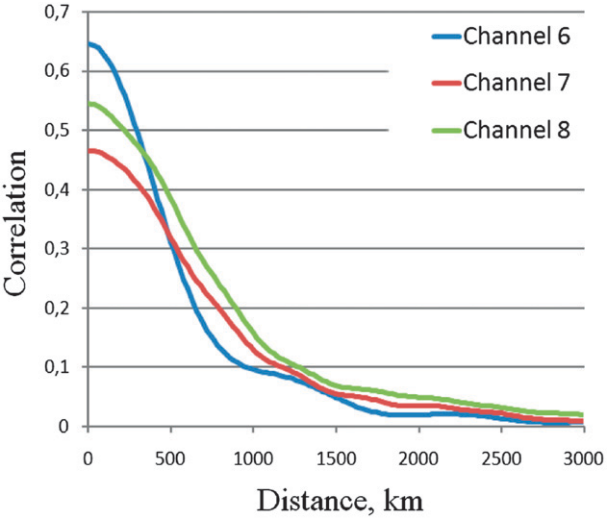

FIG. 4. Satellite c' vs forecast cross correlations.

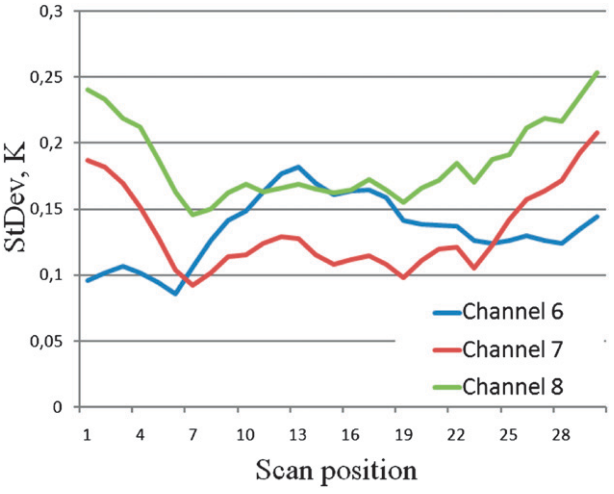

FIG. 5. The scan position dependence of the correlated satellite error standard deviation.

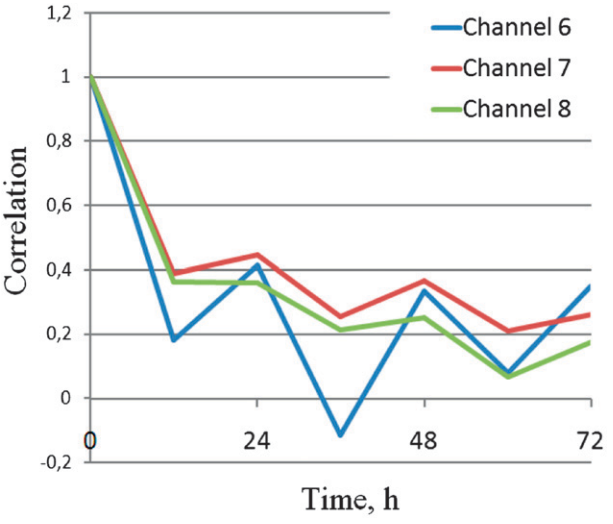

FIG. 6. Temporal satellite-minus-radiosonde correlations.

easily accessible, see Fig. 6. A significant decrease in correlation on the time scale of 1 day is clearly visible. We can comment that this decorrelation time is consistent with the about 1000-km horizontal decorrelation length scale shown in the previous figures. The origin of nonzero correlations at large lags remains unclear. Oscillations in temporal correlations seen in Fig. 6 can be explained by the impact of the diurnal cycle in the lower troposphere on the low-peaking channels (the oscillations are seen to be maximal for channel 6 and minimal for channel 8).

g. *One-point statistics: Summary*

Finally, in Table 1, we display standard deviations $\sigma_u = \sqrt{\mathbb{D}u'}$, $\sigma_c = \sqrt{\mathbb{D}c'}$ (both averaged over all scan positions), and $\sigma_f = \sqrt{\mathbb{D}f'}$, along with the cross correlation between c' and f'. Note that values of σ_u presented in Table 1 are not far from the respective instrumental error standard deviation (NEΔT) indicated in Goldberg et al. (2001): 0.15, 0.13, and 0.14.

We note that we now have threefold indirect evidence that u' can be associated with the instrumental satellite observation noise s'_{inst}. First, u' has zero interchannel cross correlations (section 6b). Second, $\mathbb{D}u'$ does not depend on the scan position (section 6d). And third, $\mathbb{D}u'$ is close to NEΔT.

7. Statistical significance

a. *Theory*

To find out how reliable the estimated covariances are and, in particular, to answer the question "is the difference of the estimated covariances from zero statistically significant?", we apply a kind of parametric bootstrap (e.g., Efron and Tibshirani 1993). Only horizontal autocovariances are examined.

Recall that for any channel, we estimate the vector of spectral variances: $\lambda := (a_0, a_1, \ldots, a_N)$. To set up the bootstrap computations, we take the estimated (using real-world data) λ as the "truth." Given this truth, we simulate all the satellite minus radiosonde differences:

$$y_p := s_p - r_p = s'_p - r'_p = c'_p + u'_p - r'_p \qquad (21)$$

for all real-world collocations $p = 1, 2, \ldots, P$ in our archive as follows. Here u'_p and r'_p are independent zero-mean random variables with variances $\mathbb{D}u'$ and $\mathbb{D}r'$, respectively; the variances are assumed to be known (we take our estimate of $\mathbb{D}u'$ and the a priori $\mathbb{D}r'$, see the appendix). So, u'_p and r'_p are readily simulated using a Gaussian pseudorandom number generator. Here c' is a random field on the sphere, so, for any time instant, it can be expanded in the following series (e.g., Yaglom 1987):

$$c'(\theta, \varphi) = \sum_{n=0}^{N} \sum_{m=-n}^{n} c_n^m Y_n^m(\theta, \varphi), \qquad (22)$$

where n is the total and m the zonal wavenumber, Y_n^m is the spherical harmonic, and θ and φ are spherical coordinates (colatitude and longitude, respectively).

TABLE 1. One-point estimates.

Channel	σ_u	σ_c	σ_f	Corr(c', f')
6	0.12	0.15	0.13	0.65
7	0.14	0.14	0.12	0.47
8	0.17	0.18	0.14	0.55

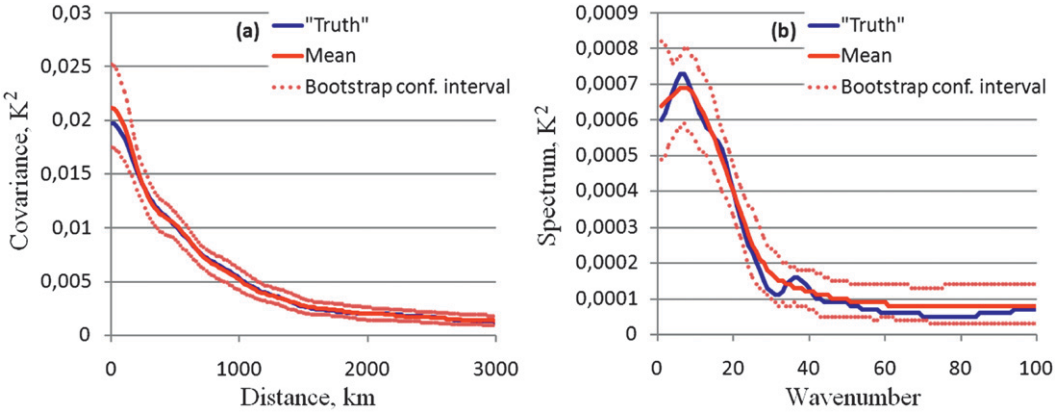

FIG. 7. 90% bootstrap confidence intervals for channel 7: (a) autocovariance and (b) autospectrum.

Neglecting here the deviations of the $c'(\theta, \varphi)$ covariances from isotropy due to scan-position dependence implies that c_n^m are all mutually independent zero-mean Gaussian random variables with variances $\mathbb{D}c_n^m = 4\pi/(2n+1)a_n$ (e.g., Yaglom 1987). So, pseudorandom realizations of the spectral coefficients c_n^m can, again, be easily generated using a Gaussian random number generator. Being substituted into Eq. (22), they give rise to independent pseudorandom realizations of the random field $c'(\theta, \varphi)$. Finally, we compute $c'(\theta, \varphi)$ at all satellite-radiosonde collocation points in our archive (labeled by p) and utilize Eq. (21) to build the simulated $s - r$ differences y_p.

After the simulated $s - r$ differences archive is built, the developed estimator is applied to it, producing the estimate $\hat{\lambda}$. The process is repeated N_b times yielding the bootstrap sample $\{\hat{\lambda}\}$, $l = 1, 2, \ldots, N_b$. The basic principle of bootstrap is that the probability distribution of $\hat{\lambda}_l - \lambda$ can be used as a proxy to the distribution of the estimation errors for the estimator in question. So, the distribution of the estimation error can be assessed.

Specifically, having N_b estimates $\{\hat{a}_n(l)\}, l = 1, \ldots, N_b$, we convert them, along with the "true" spectrum $\{a_n\}$ from spectral to physical space, see Eq. (14). Thus, we obtain N_b estimates of both the c' wavenumber variance spectrum and its covariance function. Taking advantage of the fact that in these bootstrap simulations, the truth is exactly known, we can readily assess the bias, the variance, and the confidence intervals for the estimation errors in physical as well as in spectral space.

b. Results

The true covariance function and variance spectrum for the arbitrarily selected channel 7 are denoted in Fig. 7 by the blue curves. The bootstrap-sample means are represented by the solid red curves. The difference between the "mean" and the truth curves can be used as a measure of the estimation *bias* (the systematic error). One can see that this bias is, generally, very small, with two exceptions. First, the estimated spectrum is slightly biased being smoother than the true one—as expected due to the presence of the term J_{smo} in our estimator. Second, a small bias is seen in the covariance function at small distances.

In principle, these biases can be used to correct our real-world estimates. However, we refrain from doing so for three reasons. First, the biases are much smaller than the random estimation error component quantified by the bootstrap confidence interval width (see the next paragraph). Second, our estimation technique can have biases due to inadequacies in our models of satellite and radiosonde errors. For example, the estimates can be biased as a result of unaccounted for latitudinal dependence of satellite-error statistics or inaccurate prior estimate of radiosonde error variance, etc. We believe these potential biases are small enough, but their sheer existence (inevitable because any model of nature is not perfect) implies that correcting *small* biases revealed by the above bootstrap procedure makes little sense. The third reason to not bias correct our estimates is the desire to make our technique as transparent as possible.

Furthermore, for any horizontal distance and wavenumber, we find the lower and the upper 5% points in the bootstrap sample (denoted by the dashed curves in Fig. 7) for both the estimated covariances and variance spectrum, getting 90% bootstrap confidence intervals. Being combined for all distances, Fig. 7a, and wavenumbers, Fig. 7b, the confidence intervals result in 90% "confidence strips" for the covariance and the spectrum, respectively. One can see that these confidence strips are quite narrow and never intersect the abscissa axes (the same conclusion holds for other channels, not shown). This latter fact implies, in particular, that the differences of the horizontal covariances from zero are statistically

significant. So, the estimated horizontal satellite error covariances (and spectra) can be trusted.

Besides this very important conclusion, one can see that the width of the 90% confidence strip becomes larger at small distances (as a result of scarcity of the radiosounding network), see Fig. 7a, and for small wavenumbers (because the distribution of high-quality radiosondes over the globe is far from uniform and there are few radiosonde pairs at very large distances), see Fig. 7b.

As an aside, we notice that from Fig. 7b it is seen that the bulk of the satellite-error spectrum is confined to the wavenumber range $n = 0 \div 30$.

8. Examination of unaccounted-for factors

In this section, we are going to answer the very important question: could our estimation results be obtained if, in reality, there were no satellite observation-error correlations? In any uncontrolled experiment, it is always possible that the outcome is caused not by the factor in question but by some unaccounted-for factor. In our case, the estimated satellite-minus-radiosonde correlations can, in principle, be due to not only satellite error correlations, but also due to a number of error sources, which we intend to check in this section. In statistical terms, in order to draw justified conclusions about satellite correlations on the basis of the above statistics, we have to reject the ''null hypothesis'' of zero satellite correlations.

First, we reject the possibility of serious program bugs by analyzing the bootstrap simulations. Second, we simulate various real-world error sources and check whether or not they can induce multivariate correlations comparable to what we have estimated using real data. Third, we check the impact of the bias-correction scheme.

a. Self-checking the estimation procedure by using simulated observations

The results of the bootstrap simulations presented in section 7 indicate that our estimator works properly. Indeed, with simulated data, the specified error covariances are reproduced very well, which can be seen in Fig. 7 by comparing the truth and the estimated mean curves.

We also perform a ''white noise'' check, in which we simulate spatially uncorrelated satellite errors. The outcome of this test is that the estimated spatial correlations turn out to be really close to zero (not shown). This implies that our estimation procedure cannot produce significant horizontal correlations ''out of nothing.''

Thus, the satellite covariances we have estimated cannot be caused by potential program bugs in the estimation scheme.

b. Roles of radiosonde radiation and inertia errors

Radiosonde observation errors are the first thing that comes to mind as a potential source of horizontal and temporal satellite-minus-radiosonde correlations.

To the best of our knowledge, there are two sources of potentially horizontally correlated errors for radiosonde observations: radiation error and inertia error.

As for the radiation error (caused by heating of the sensor by the sun) we examine its influence by comparing daytime versus nighttime $s - r$ horizontal covariances. The justification for this approach is that at night, there is no heating by the sun and so no radiation error. For the best radiosonde types used in this study, the day–night contrasts in the estimated covariances appear to be negligible (not shown). So, the radiation radiosonde error plays negligible role in building the satellite-minus-radiosonde covariances.

The inertia (lag) error is due to the finite inertia of the radiosonde sensor, so that, roughly speaking, the measurement was actually done τ seconds prior to the reported observation time. For Vaisala sondes, τ is less than 0.4 s at 1000 hPa, 1 s at 100 hPa, and 2.5 s at 10 hPa (this information is available online at www.vaisala.com). The three examined AMSU-A channels peak at about 350, 250, and 150 hPa, respectively (e.g., Goldberg et al. 2001), so the typical τ there can be assessed as 0.7 s. If we assume that the mean ascent velocity is 6 m s^{-1} and the absolute value of the vertical temperature gradient is 6.5 K km^{-1}, then the inertia temperature error appears to be about 0.03 K. In terms of error variance, this is less than 0.001 K^2, which is 20–40 times less than the estimated correlated satellite observation error variances.

Thus, radiosonde measurement errors cannot lead to spatial and temporal satellite-minus-radiosonde covariances we found in this study.

c. Roles of the surface and the upper stratosphere

Another potential source of the spatiotemporal correlations is the boundary effects: if the uncertainties in the state of the underlying surface or of the stratosphere above the radiosonde top do significantly affect $\mathcal{H}(\mathbf{X}^{\text{raob}})$ and do correlate in space and time, then satellite minus radiosonde differences can become correlated as well.

For all satellite data in our archive of satellite-radiosonde collocations, we deliberately change the land surface emissivity from 0.8 to 0.6 and from 0.8 to 0.99 and find quite small impacts: the resulting error variances are 0.002 K^2 for channel 6 and less than 10^{-5} K^2 for channels 7 and 8.

Next, we assess the impact of the stratospheric uncertainty above 10 hPa by imposing the constant perturbation

of 5 K there and looking at the effect on $\mathcal{H}(\mathbf{X}^{\text{raob}})$. In terms of the additional error variance, the effect is as large as 0.015 K^2 for channel 9 (which was the main reason to exclude this channel from our study), and quite small for channels 6, 7, and 8: less than 0.001, 0.001, and 0.002 K^2, respectively.

So, neither the surface nor the upper-stratospheric uncertainties are responsible for the estimated error covariances.

d. Role of the observation operator's nonlinearity

In defining the errors in radiance space (section 3a), linearity of $\mathcal{H}$ is used. We note that if $\mathcal{H}$ were significantly nonlinear, then $r' = \mathcal{H}(\mathbf{X} + \delta\mathbf{X}) - \mathcal{H}(\mathbf{X})$ (where $\delta\mathbf{X} := \delta\mathbf{X}^{\text{raob}}_{\text{inst}} + \delta\mathbf{X}^{\text{raob}}_{\text{repr}}$) could become correlated in space/time as a result of the respective correlations for $\mathbf{X}$ and thus induce spatiotemporal correlations for the $s - r$ differences we study. Here, the validity of the linearity hypothesis is checked.

Similarly to the previous subsection, we evaluate the variance of the linearization error involved in Eq. (9). To this end, we impose, to $\mathbf{X}^{\text{raob}}$, a random perturbation $\Delta\mathbf{X}$ with independent values at different levels and with standard deviation equal to 2 K (an upper bound for radiosonde error standard deviation). Then, we examine the linearization error, $\Delta r - dr$, where $\Delta r := \mathcal{H}(\mathbf{X}^{\text{raob}} + \Delta\mathbf{X}) - \mathcal{H}(\mathbf{X}^{\text{raob}})$ and $dr := \mathbf{H} \cdot \Delta\mathbf{X}$. Its variance is evaluated using real profiles of $\mathbf{X}^{\text{raob}}$ and appears to be as small as 10^{-4} K^2.

The same very small upper bound is found for the linearization error involved in the definition of the forecast error in radiance space $f' = \mathcal{H}(\mathbf{X}^f) - \mathcal{H}(\mathbf{X})$. We tried different vertical perturbations (a constant and a sinusoid—besides the white noise) with almost the same result. So, the linearization errors cannot give rise to the error variances, and hence, covariances we found.

e. Impact of the representativeness errors

As noted in section 3a, for the three sources of information we use in this study: satellite, radiosonde, and forecast, the degree of spatiotemporal averaging as well as locations of the observation points are somewhat different. This introduces representativeness errors. Their influence on our statistics is checked here.

1) HORIZONTAL AND TEMPORAL REPRESENTATIVENESS ERRORS

The horizontal collocation radius R_{coll} and the temporal window width T_{coll} are chosen with the intention to make the horizontal and temporal parts of the above representativeness error comparable. Indeed, the AMSU-A field-of-view diameter is about 50–100 km ($\simeq R_{\text{coll}}$). Furthermore, a radiosonde lifts to the peaks of channels' 6–8 weighting functions (100–400 hPa) a considerable amount of time, 0.5–1 h, and moves, thereby, 30–70 km away from the launch site (with the mean horizontal wind 20 m s^{-1}). The 1° resolution of forecast fields implies 55–110-km averaging in midlatitudes. Interpolation from the forecast grid to a subsatellite or radiosonde point involves interpolation from the nearest grid points 30–55 km away. So, we see that all involved uncertainties in space and time for s, r, and f are more or less mutually consistent, because for the atmospheric statistics, 50 km in the horizontal roughly corresponds to 1 h in time.

With these scales of uncertainties (50 km and 1 h), we can be sure that they cannot cause 1000-km-wide correlations we found. To experimentally assess the impact of temporal representativeness errors, the $s - r$ covariances are compared for two time windows, $T_{\text{coll}} =$ 1 h and $T_{\text{coll}} = 2$ h. The differences appeared to be not significant (not shown). Consequently, the role of temporal as well as horizontal representativeness errors in this study in negligibly small.

2) VERTICAL REPRESENTATIVENESS ERRORS

To reduce the vertical part of the representativeness error caused by the finite vertical resolution of radiosonde data, we opt (on the basis of experiments, not shown) to use radiosonde geopotentials rather than temperatures because geopotential is a vertically integrated variable and so is less susceptible to representativeness error. The remaining vertical representativeness error exists in the form of the error of the vertical interpolation from the relatively coarse grid of mandatory radiosonde levels to the RTTOV grid.

To evaluate the role of this latter error source, we make use of 16 arbitrarily selected high-resolution radiosonde profiles, in which data are sampled every 10 s (about 60 m in the vertical). Then, we apply RTTOV to both fine-grid (high-resolution temperature data) and coarse-grid (mandatory levels of geopotential and humidity) radiosonde profiles. The coarse-grid geopotential profiles are computed by integrating the hydrostatic equation using temperature and humidity on the fine grid. To transform both fine-grid and coarse-grid radiosonde profiles to the RTTOV vertical grid, we use piecewise-linear in log pressure interpolation for both temperature and humidity. For coarse-grid profiles, temperatures are obtained from geopotential first on intermediate levels (using hydrostatics) and then linearly interpolated to the RTTOV levels.

The resulting mean-squared differences between high- and low-resolution radiosonde data in radiance space equal 0.005, 0.002, and 0.002 K^2 for channels 6, 7, and 8, respectively. As above, these are very small numbers as

compared with the correlated satellite error variances (only for channel 6, the noise reaches 1/4 of the signal in variance).

f. Impact of the bias-correction scheme

In this subsection, we show that potential problems in the bias-correction scheme that lead to incorrect bias-correction coefficients cannot cause the horizontal covariances we found. We examine only the state-dependent bias predictors, which can be deemed to introduce some spatial correlations in the data: $Z_1 = Z_{850}^{300}$ and $Z_2 = Z_{200}^{50}$. The constant predictor, $Z_3 = 1$, is mentioned here for the sake of generality. As noted in section 5, the observation itself as a predictor appears to have little impact on our estimates and so it is dropped here.

Our bias-correction scheme transforms satellite observation before bias correction s_{bbc} to bias-corrected data s:

$$s = s_{\mathrm{bbc}} - \sum_{i=1}^{3} b_i Z_i. \tag{23}$$

Now, suppose that for some channel, our scheme contains an error: b_i are wrong—in contrast to the correct scheme (with weights b_i^*). Suppose, further, that with the correct scheme, there are no horizontal (s', s') covariances at all: the covariances we found are exclusively due to wrong b_i. Then, after simple algebra, we find that the $s - r$ differences we use in the estimation of horizontal covariances become

$$s - r = s' - r' + \sum (b_i^* - b_i) Z_i. \tag{24}$$

In this equation, the correct-scheme's observation error s' is, by supposition, horizontally uncorrelated and so is r' [assumption (i) in section 3b], so the only source of horizontal correlations for $s - r$ is the term $\sum (b_i^* - b_i) Z_i$. In this term, the third predictor (a constant) cannot cause any covariances, so these should be, thus, due to the residual, $\psi := w_1 Z_1 + w_2 Z_2$, where $w_i = b_i^* - b_i$. Therefore, there exist real numbers w_1 and w_2 such that the resulting ψ explains the horizontal correlations we found (i.e., its correlations should fall to 0.25 at the distance of about 1000 km).

The problem with this statement is that both $Z_1 = Z_{850}^{300}$ and $Z_2 = Z_{200}^{50}$ have much greater horizontal length scales (not shown), so neither of them alone can give rise to length scales of about 1000 km. But, maybe, there is a linear combination of Z_1 and Z_2 that can? We tried a number of linear combinations and found that they all have quite similar horizontal covariances, with a bit smaller length scale for $Z_1 + Z_2$, whose covariances estimated at the collocation points with our basic estimator are depicted in Fig. 8. One can see that even these narrowest covariances are 2–3 times as wide as our real-world estimates (cf. Fig. 1). This implies that erroneous bias-correction coefficients cannot give rise to the horizontal covariances we found for real data. So, the estimated satellite error covariances are not caused by a potential problem in the bias-correction scheme.

Summarizing, we have studied the roles of all non-satellite error sources we were able to point out as possible causes of the correlations we found. Neither of these error sources and even these all combined cannot explain the estimated satellite-minus-radiosonde correlations. So, we are allowed to attribute the estimated covariances to satellite observation errors and thus reject the null hypothesis of zero satellite correlations.

9. Comparison of our estimates with those by Bormann and Bauer (2010)

Here, we discuss why our conclusions (which imply that there are strong multiple correlations for AMSU-A data) disagree with the conclusions by Bormann and Bauer (2010) (who state that there are no significant AMSU-A error correlations).

The results reported in (Bormann and Bauer 2010) were obtained using three techniques. The first one (referred to as the Lönnberg–Hollingsworth method there) is exactly the same technique we use to estimate the uncorrelated satellite error variance. And we note that our results are here consistent with those by Bormann and Bauer (2010).

Their second and third techniques heavily rely on the assumption that satellite errors do not correlate with forecast errors. Our statistics, however, imply that these cross correlations are quite strong, see Fig. 4 and Table 1. We claim that if we neglected satellite-versus-forecast cross correlations, our conclusions would become very similar to those by Bormann and Bauer (2010).

Indeed, let us, following Bormann and Bauer (2010), subtract our estimates of forecast-error covariances, $(f - r, f - r)$, from satellite-minus-forecast covariances, $(s - f, s - f)$; both are plotted in Fig. 1, see the middle and the bottom panels, respectively. The results are shown in Fig. 9, together with the dots at zero distance that represent our estimates of $\mathbb{D}u'$.

One can see in Fig. 9 that neglecting cross correlations between satellite and forecast errors almost completely removes the horizontal satellite error covariances in our statistics. This suggests that our finding that cross correlations between satellite and forecast errors are important, dramatically changes the conclusions on AMSU-A error correlations; otherwise, our statistics do not contradict to those by Bormann and Bauer (2010).

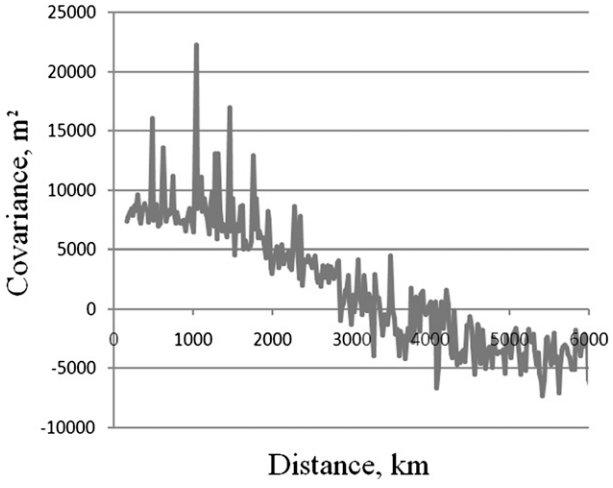

FIG. 8. Horizontal covariances for $Z_1 + Z_2$.

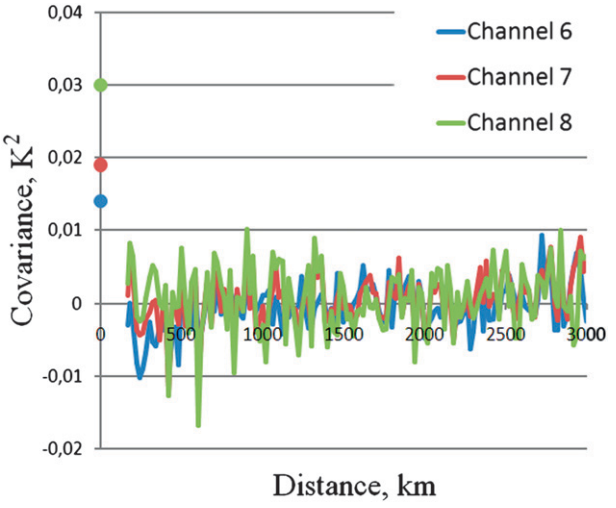

FIG. 9. Difference of satellite-minus-forecast covariances and forecast-error covariances. The dots at the zero distance represent estimates of uncorrelated satellite variances.

10. The main findings

- The AMSU-A error can be modeled as a sum of two mutually uncorrelated components: the correlated c' and the uncorrelated u' components; the uncorrelated error can be associated with the instrumental satellite error. It has no interchannel cross-correlations. Its standard deviation $\sqrt{\mathbb{D}u'}$ for each channel is almost independent of the scan position and appears to be close to the nominal observation noise standard deviation NEΔT.
- The correlated AMSU-A error can be associated with the (bias corrected) forward-model error. Its standard deviation $\sqrt{\mathbb{D}c'}$ is found to depend on the scan position (zenith angle).
- Horizontal AMSU-A (channels 6–8) error correlations appear to be quite broad, falling to the 25% level at distances as large as about 1000 km. These correlations appear to be directionally isotropic.
- Interchannel AMSU-A correlations have horizontal structures similar to those for autocorrelations. At zero distance, cross correlations of the correlated part of the satellite errors are as large as 0.5–0.8 for the adjacent channels and fall to 0.25 for the nonadjacent pair of channels (6, 8).
- There are significant cross correlations between background (forecast) errors and the correlated part of AMSU-A errors. These cross correlations, to the best of our knowledge, have not been considered so far in practical data assimilation. At zero distance, they turn out to be as large as 0.45–0.65. Their horizontal length scales are, again, similar to those for autocorrelations.
- There are significant temporal AMSU-A error correlations on the time scale of about 1 day.

Statistical significance of the horizontal satellite error correlations is established using the bootstrap technique.

Nonsatellite potential sources of spatial and other correlations are studied and found to be not responsible for the error correlations found in this study. So, we believe our conclusions on satellite error correlations can be trusted.

11. Implications for practical data assimilation

In the authors' opinion, all the above observation error correlations need to be accounted for in practical data assimilation schemes. Palliative solutions like variance inflation plus data thinning are, in general, not desirable because they, effectively, act to compensate one incorrectness of the observation error covariance model (no error correlations) by another one (the increased error variance). We believe that pushing the error model more and more away from the truth can preclude further progress in assimilation of observations. Besides, data thinning reduces the spatial resolution of satellite data, which can be not desirable in mesoscale data assimilation.

Temporal correlations and cross correlations between observation and forecast errors deserve special attention. Addressing these rather unusual correlations will require reformulation of the data assimilation equations and is achievable, most likely, in Kalman filter–like schemes. These kinds of error correlations can be expected to exist for any voluminous observations with spatial/temporal error correlations: not only for various satellite observation types, but also for radar data.

Our results are obtained for only a small fraction of all satellite channels (6–8 for AMSU-A), so in practical applications these results need to be extrapolated to other channels, for which the satellite-minus-radiosonde technique is not applicable. This extrapolation can be ad hoc, but at least we know which error correlations are to be expected.

Acknowledgments. This study was partially supported by the Consortium for Small-Scale Modeling (COSMO). We thank A. P. Kats for providing us with high-resolution radiosonde data and consulting on properties of radiosounding observations. The valuable comments of two anonymous reviewers were helpful in improving the manuscript.

APPENDIX

The Bootstrap-Based Estimator

Here, we describe a simulation-based technique devised to optimize the weight of the J_0 term in our estimator Eq. (18) and properly account for the uncertainty of the specified radiosonde error variance $\mathbb{D}r'$.

We assess $\mathbb{D}r'$, very roughly, as one-half of the averaged (over the whole archive) radiosonde-minus-background variance (in terms of each AMSU-A channel's brightness temperature). The uncertainty of this rough estimate $\hat{\mathbb{D}}r'$ is accounted for by specifying the appropriate weight w_0 of the term J_0 (section 4c) as follows.

We assume that the true $\mathbb{D}r'$ is a random variable uniformly distributed over the subjectively selected range from $(0.7\hat{\mathbb{D}}r'$ to $1.3\hat{\mathbb{D}}r')$. We simulate $N_b = 100$ pseudorandom realizations of the ''true'' $\mathbb{D}r'$. Next, conditionally on $\mathbb{D}r'$, for each its realization and postulating both the true u' variance and the true c' variance spectrum (as it is described in section 7), we simulate the whole archive of satellite-minus-radiosonde differences (at their real locations).

Then, we fix w_0 [see Eq. (17)] somewhere within its plausible range and, for each of the N_b realizations, apply our full estimator, Eq. (18), and compare the estimated satellite error spectrum $\hat{a}_n$ with the true one a_n. The resulting misfit is measured by a norm $\|\hat{a}_n(l) - a_n(l)\|$ that involves averaging over both the wavenumbers, $n = 0, \ldots, N$, and the bootstrap sample, $l = 1, \ldots, N_b$ (not shown). Finally, we let w_0 vary, repeat the whole process for a number of w_0 values, and select w_0 that yields the smallest estimation error $\|\hat{a}_n(l) - a_n(l)\|$.

Thus, we have described the technique that allows us to optimize our estimator (specifically, the weight of the zero-distance term J_0) using bootstrap.

REFERENCES

Bormann, N., and P. Bauer, 2010: Estimates of spatial and interchannel observation-error characteristics for current sounder radiances for numerical weather prediction. I: Methods and application to ATOVS data. *Quart. J. Roy. Meteor. Soc.,* **136,** 1036–1050.

——, S. Saarinen, G. Kelly, and J.-N. Thépaut, 2003: The spatial structure of observation errors in atmospheric motion vectors from geostationary satellite data. *Mon. Wea. Rev.,* **131,** 706–718.

Dando, M., A. Thorpe, and J. Eyre, 2007: The optimal density of atmospheric sounder observations in the Met Office NWP system. *Quart. J. Roy. Meteor. Soc.,* **133,** 1933–1943.

Efron, B., and R. Tibshirani, 1993: *An Introduction to the Bootstrap*. Chapman and Hall, 436 pp.

Garand, L., S. Heilliette, and M. Buehner, 2007: Interchannel error correlation associated with AIRS radiance observations: Inference and impact in data assimilation. *J. Appl. Meteor.,* **46,** 714–725.

Goldberg, M. D., D. S. Crosby, and L. Zhou, 2001: The limb adjustment of AMSU-A observations: Methodology and validation. *J. Appl. Meteor.,* **40,** 70–83.

Harris, B. A., and G. Kelly, 2001: A satellite radiance-bias correction scheme for data assimilation. *Quart. J. Roy. Meteor. Soc.,* **127,** 1453–1468.

Le Marshall, J., J. Jung, T. Zapotocny, C. Redder, M. Dunn, J. Daniels, and L. P. Riishojgaard, 2008: Impact of MODIS atmospheric motion vectors on a global NWP system. *Aust. Meteor. Mag.,* **57,** 45–51.

Liu, Z.-Q., and F. Rabier, 2003: The potential of high-density observations for numerical weather prediction: A study with simulated observations. *Quart. J. Roy. Meteor. Soc.,* **129,** 3013–3035.

Okamoto, K., M. Kazumori, and H. Owada, 2005: The assimilation of ATOVS radiances in the JMA global analysis system. *J. Meteor. Soc. Japan,* **83,** 201–217.

Saunders, R. W., M. Matricardi, and P. Brunel, 1999: An improved fast radiative transfer model for assimilation of satellite radiance observations. *Quart. J. Roy. Meteor. Soc.,* **125,** 1407–1425.

Stewart, L., J. Cameron, S. Dance, S. English, J. Eyre, and N. Nichols, 2009: Observation error correlations in IASI radiance data. Mathematics Rep. Series 1/2009, University of Reading, Reading, United Kingdom, 26 pp.

Uppala, S. M., and Coauthors, 2005: The ERA-40 re-analysis. *Quart. J. Roy. Meteor. Soc.,* **131,** 2961–3012.

Yaglom, A. M., 1987: *Correlation Theory of Stationary and Related Random Functions. Vol. 1: Basic Results*. Springer, 526 pp.

Zapotocny, T. H., J. A. Jung, J. F. L. Marshall, and R. E. Treadon, 2008: A two-season impact study of four satellite data types and rawinsonde data in the NCEP global data assimilation system. *Wea. Forecasting,* **23,** 80–100.